Journal of Anatomy

J. Anat. (2014) **225**, pp209–219 doi: 10.1111/joa.12200

Functional anatomy and feeding biomechanics of a giant Upper Jurassic pliosaur (Reptilia: Sauropterygia) from Weymouth Bay, Dorset, UK

Davide Foffa,[1] Andrew R. Cuff,[1] Judyth Sassoon,[1] Emily J. Rayfield,[1] Mark N. Mavrogordato[2] and Michael J. Benton[1]

[1]*School of Earth Sciences, University of Bristol, Bristol, UK*
[2]*μ-VIS CT Imaging Centre, Engineering Sciences, University of Southampton, Southampton, UK*

Abstract

Pliosaurs were among the largest predators in Mesozoic seas, and yet their functional anatomy and feeding biomechanics are poorly understood. A new, well-preserved pliosaur from the Kimmeridgian of Weymouth Bay (UK) revealed cranial adaptations related to feeding. Digital modelling of computed tomography scans allowed reconstruction of missing, distorted regions of the skull and of the adductor musculature, which indicated high bite forces. Size-corrected beam theory modelling showed that the snout was poorly optimised against bending and torsional stresses compared with other aquatic and terrestrial predators, suggesting that pliosaurs did not twist or shake their prey during feeding and that seizing was better performed with post-symphyseal bites. Finite element analysis identified biting-induced stress patterns in both the rostrum and lower jaws, highlighting weak areas in the rostral maxillary-premaxillary contact and the caudal mandibular symphysis. A comparatively weak skull coupled with musculature that was able to produce high forces, is explained as a trade-off between agility, hydrodynamics and strength. In the Kimmeridgian ecosystem, we conclude that Late Jurassic pliosaurs were generalist predators at the top of the food chain, able to prey on reptiles and fishes up to half their own length.
Key words: beam theory; finite element analysis; Kimmeridgian; Pliosauridae; Pliosauroidea.

Introduction

Pliosauroidea (Plesiosauria, Sauropterygia) is a group of secondarily marine reptiles; their fossil record spans the Mesozoic from the Late Triassic to Late Cretaceous, some 150 Myr. Towards the end of the Early Jurassic, pliosauroids achieved global distribution and their highest diversity (Ketchum & Benson, 2010). Many studies have considered the taxonomy, body shape, ecology and locomotion of pliosaurs, but fewer have concentrated on feeding strategies, and they are mainly based on tooth-shape analogies with extant forms, direct fossil evidence including gut contents, and bite marks. The functional anatomy of the pliosaur skull has been studied in a few large specimens – *Rhomaleosaurus zetlandicus* (Toarcian, Early Jurassic; Taylor, 1992), *Pliosaurus westburyensis*. (Kimmeridgian, Late Jurassic; Taylor & Cruickshank, 1993), Pliosauridae gen. et sp. nov. (Barremian, Early Cretaceous; M. Gómez-Pérez, unpublished communication), *Kronosaurus queenslandicus* (Albian-Aptian, Early Cretaceous; McHenry, 2009) – but 3D functional models are provided only for the last two taxa, in unpublished work. These analyses suggest that, particularly for *Pliosaurus,* large size alone allowed these reptiles to produce enough force to dismember and/or entirely swallow their prey items without relying on specific mechanical adaptations (Taylor, 1987, 1992; Taylor & Cruickshank, 1993; Martill et al. 1994). Stomach contents and evaluations of size and proportions of the dentition depict pliosaurs as top predators; in particular, deep tooth roots and thick tooth crowns can be seen as adaptations to resist strong feeding forces and thus considerably enlarge the dimensional spectrum of possible prey (Massare, 1987; Martill et al. 1994). Based on gut contents, analogies with modern mammals, tooth shape, and inferred diet, pliosaurs have been classified in different guilds, namely, cutting, piercing and a combination of both ('generalist') (Massare, 1987). It was assumed that the largest pliosaurs could procure prey of any size. However, from a kinematic perspective, the dimension of the akinetic pliosaur skull sets a physical limit to the size of each mouthful.

The discovery of a new, exceptionally large well-preserved skull of a Late Jurassic (Kimmeridgian) pliosaur in

Correspondence
Davide Foffa, School of Earth Sciences, University of Bristol, Wills Memorial Building, Queen's Road, Bristol BS8 1RJ, UK.
E: df1818@my.bristol.ac.uk

Accepted for publication *22 April 2014*
Article published online *13 June 2014*

Weymouth Bay, Dorset, UK (DORCM G.13 675), recently assigned to *Pliosaurus kevani* (Benson et al. 2013), provides an opportunity to test these suggestions by applying numerical biomechanical techniques. Here we reconstruct and test the functional anatomy and feeding performance of *P. kevani* by (i) reconstructing adductor muscle anatomy to provide an estimate of jaw muscle and bite forces; and (ii) testing whether the skull is better adapted to twisting or shaking as a means of dismembering prey (Taylor, 1987) using a comparative beam theory analysis and finite element analysis (FEA).

Institutional abbreviations

DORCM, Dorset County Museum, Dorchester, UK; FMNH, Field Museum of Natural History, Chicago, USA; NHMUK, Natural History Museum, London, UK; OUVC, *Ohio University Vertebrate Collection*; TMM, Texas Memorial Museum, Austin, TX, USA.

Material and methods

DORCM G 13 675 is a nearly complete and mostly undeformed pliosaur skull, roughly 2 m long (mandibular length) and 80 cm wide at the jaw joints (Fig. 1). It is one of the largest pliosaurs ever found, rivalling the dimensions of *Pliosaurus funkei* (Knutsen et al. 2012) from Svalbard and the 'Aramberri monster' (Pliosauridae indet.) from Mexico (Buchy, 2003).

The specimen was subjected to computed tomography (CT) scanning at the 'μ-VIS' Centre for Computed Tomography (University of Southampton), using a custom-built Nikon 450 kV micro-focus X-CT system. The specimen was scanned in sections and the resolution varies from 1.0815 to 0.5066 (mm per pixel) and slice thickness between 1.5 mm (premaxillae) and 3 mm for all segments (see Supporting Information Table S1). The CT scans were processed, re-aligned and digitally restored using AVIZO® (versions 6.1.1, 6.3 and 7.0.1; VSG, France). The specimen lacked the mandibular symphysis; this was digitally reconstructed using stereo-photogrammetry (Falkingham, 2012) on a cast model and processed with AUTODESK® 123D CATCH and AVIZO.

Despite being almost complete, the DORCM G 13 675 specimen lacks further bony elements, especially in the postorbital region and lower jaws, which had to be reconstructed. In particular, parts of the pterygoids, quadrates, squamosal and jugals are missing; the lower jaws are incomplete, lacking the mandibular symphysis, with minor damage on the ventral surface of the left ramus, and the right articular, which did not fit the scanner field of view during the CT-scanning process. Consequently, missing or damaged parts were digitally replaced by mirroring the equivalent symmetric counterparts or reconstructed (as in Lautenschlager, 2013). In particular, part of the pterygoids, the squamosals, the quadrates and paraoccipital were digitally created based on photographs and diagrams of *Kronosaurus, Liopleurodon*, *P. westburyensis* and *Pliosaurus carpenteri* (specimens BRSMG Cc332 and BRSMG Cd6172; Taylor, 1992; Taylor & Cruickshank, 1993; L. F. Noè, unpubl. comm.; McHenry, 2009; Sassoon et al. 2012). The quadrate-articular geometry was also based on the literature available but mainly on three-dimensionally preserved pliosaurid specimens displaying jaw and skull in life-anatomical connection. These are: an unidentified

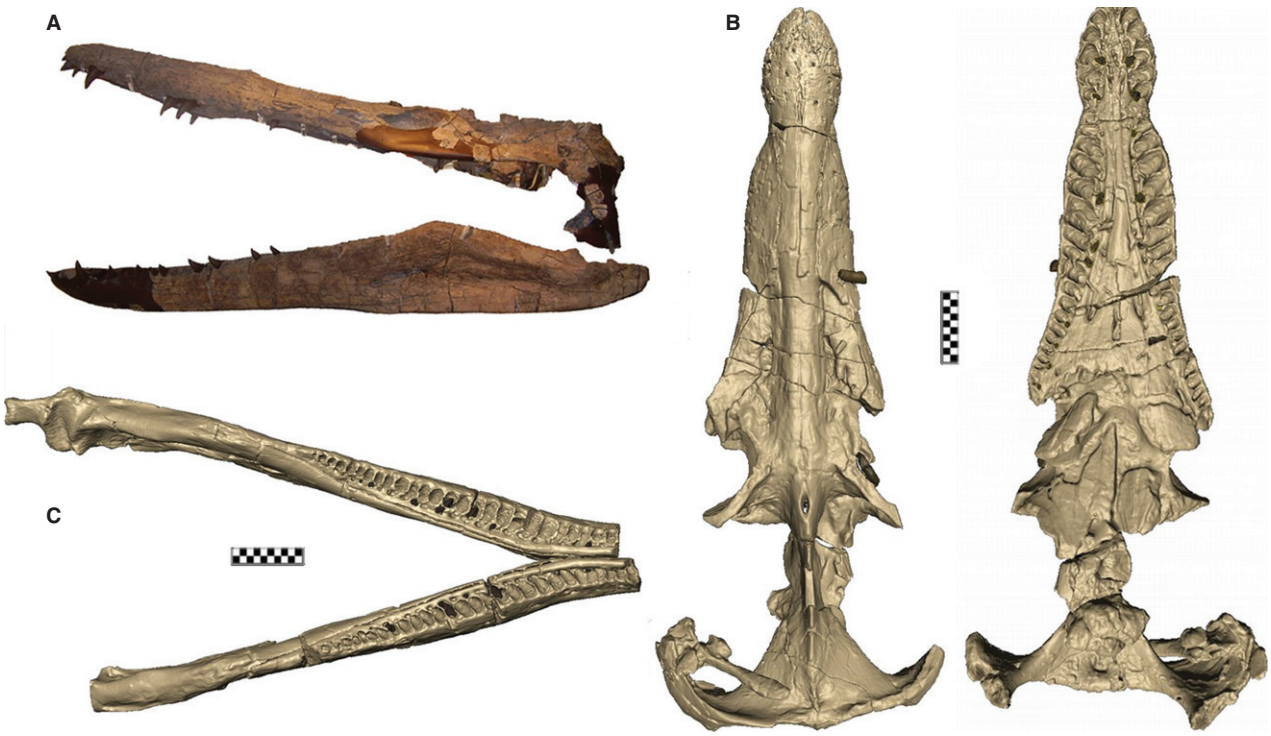

Fig. 1 DORCM G.13 675 skull and digital models. (A) Skull and lower jaws, left lateral view; (B) CT reconstruction of the original skull, dorsal and ventral view; (C) lower jaws, dorsal view. Scale bar: 20 cm.

Kimmeridgian pliosaurid specimen hosted in Patrick Clarke's private collection; the final result was double-checked against *Peloneustes philarcus* and *Simolestes vorax* (specimens NHMUK R4058; NHMUK R3319; L. F. Noè, unpubl. comm.; Ketchum & Benson, 2011a) (further details are available in Supporting Information Fig. S5, and upon request to the corresponding author). Other parts were retrodeformed; in particular, the mandibular symphysis model built for the museum display was digitally stretched in the rostral direction as it was considered to be too short (after Benson et al. 2013); the parietal crest was dorsally shifted and rotated to correct for braincase compression. All modifications were produced using AVIZO v 6.0; 6.1; 7.0 (VSG).

Muscle reconstruction and bite force

Adductor musculature was digitally reconstructed using anatomical landmarks such as rugosities on the bone surface, and comparisons with models proposed in the literature for pliosaurs and archosaurs, as well as general reptilian anatomy (Romer, 1956; Gorniak et al. 1982; Taylor, 1992; Taylor & Cruickshank, 1993; Cleuren & De Vree, 2000; Holliday & Witmer, 2007; Holliday, 2009; Jones et al. 2009). Once the insertion areas were identified, 3D muscle reconstruction and bite force calculation were carried out following the procedure thoroughly described in Lautenschlager (2013) directly on the digital restored skull; in this way errors (mainly associated with volume reconstruction and lever arm length) caused by fossil deformation and scaling were avoided or minimised.

Bite forces were calculated following the 'dry skull' method, which allows quantification of the force exerted by each muscle group based on their cross-sectional area (CSA; Thomason, 1991) using the equations:

$$F_{mus} = CSA \cdot \sigma \quad (1)$$

$$F_{res} = F_{mus} \cdot \cos\alpha \cdot \cos\beta \quad (2)$$

where α and β are angles of the muscle insertions with the vertical line measured in the coronal and sagittal plan as measured from the digital model in AVIZO; F_{mus} and F_{res} respectively indicate muscle force and resistance force.

However, this method is known to underestimate bite force. Thus to obtain a minimum and a maximum value we introduced a corrective factor of 1.5 to our estimates, following Lautenschlager (2013). This factor was experimentally calculated in Thomason (1991) and is consistent with the value found by Walmsley et al. (2013), which showed that experimentally measured crocodilian bite force is 1.6 times the estimate based on the dry skull method. After digitally measuring muscle moment arms, lever theory was applied to calculate bite force at eight positions along the tooth row (1st premaxillary tooth, 1st, 23rd, last dentary tooth, unilateral and bilateral for each position). Sensitivity analyses to account for variation in the volume of the *M. pterygoideus* and muscle pennation were performed (see Supporting Information Data S1, d).

Because of the skull preservation, it was not possible to get an accurate estimate of its volume and surface area. Consequently, it was impossible to produce the recommended bite force comparisons, in which the forces are scaled to skull volume and/or surface (Dumont et al. 2009). Therefore, to compare *P. kevani* bite forces with crocodilians, the pliosaur skull was rescaled to different lengths and bite forces re-calculated with the same procedure described above. However, there are at least two reasons why, in this study, rescaling to length is acceptable: (i) we compared similar feeding styles at 'ecologically equivalent sizes' (see Snively et al. 2010; Walmsley et al. 2013); (ii) our beam theory results account for cross-sectional areas and other factors, and allow comparison of the effect of length and surface area scaling.

Finite element analysis

Digital models generated from CT scans of the whole lower jaw and the rostral part of the skull (anterior 50% of the snout) were exported into HYPERMESH v11.0 (Altair, USA), then converted into 3D meshes to perform finite element analyses (FEA). FEA is a technique that calculates the strain and stress responses to imposed loads and boundary conditions on a structure subdivided into a finite number of elements with simple geometries (Rayfield, 2007; Benton, 2010).

Eight FE-models were produced, two for the rostrum and six for the lower jaws. In the lower jaw models, we tested six different boundary conditions in order to simulate the full range of biting scenarios (Fig. 3). Constraints were applied at the articular surface (across three nodes enclosing a small area) and at six different bite positions: three unilateral bites and three bilateral bites at the 1st, 13th and 36th dentary teeth (at single nodes). Only the symphyseal suture was modelled. Forces simulating the pulling effect of a unified muscle mass posterior to the coronoid process were applied to the FE-meshes (Rayfield et al. 2001; Dumont et al. 2009; McHenry et al. 2006; Wroe et al. 2008). In the two rostrum FE-models, each node on the most caudal section of the snout was constrained and bite forces were applied either unilaterally or bilaterally at the 1st premaxillary teeth; sutures were not modelled.

The pliosaur 3D reconstructions (snout and lower jaws) were converted into a number of FE models with linear elements of differing sizes, using the 'shrink wrap' function to maintain the overall geometry. Mesh errors (duplicates, free edges, T-connections, dihedrals and other imperfections) were removed and the models were converted into 3D FE-meshes. Convergence tests were performed on five lower jaw models and three snout models with successively smaller element sizes (Bright & Rayfield, 2011).

Bone material was assigned an isotropic Young's modulus, E = 15 GPa, and Poisson ratio υ = 0.29, averages for *Alligator* cortical bone (Zapata et al. 2010). The suture properties were E = 0.09 GPa and υ = 0.3 (Porro et al. 2011; Reed et al. 2011). Each model was analysed with ABAQUS software 6.10-2 (Dassault Systèmes Simulia, Providence, RI, USA). We chose alligator bone for material properties for morphological reasons and because of their semi-aquatic lifestyle. We cannot demonstrate that this is more or less appropriate than other choices, but it is unlikely that different material properties would significantly alter the results of a comparative analysis of performance such as this (Walmsley et al. 2013).

Beam theory

A comparative analysis of resistance to bending and twisting loads was performed employing beam theory to calculate the second moment of area (I) and the polar moment of inertia (J) of successive transverse slices through the rostrum and lower jaws (Busbey, 1995). This method was successfully used to study feeding mechanics in dinosaurs and crocodilians by testing the biomechanical resistance of rostra and lower jaws (Cuff & Rayfield, 2013; Walmsley

Table 1 Comparison of force input per muscle group.

Muscle group	Cross-sectional area (cm^2)	Force (N) min	Force (N) MAX	Ratio of muscle contribution (%)
M. ame	664.25	19927	29891	47/36*
M. amp	272.82	8185	12278	19/15*
M. pst	275.48	8264	12396	19/15*
*M. pt/M. pt**	210.16/600*	6304/18 000*	9456/27 000*	15/33*
Total	—	42681/54 376*	64 012/81 564*	

*Model with rescaled *mpt.*

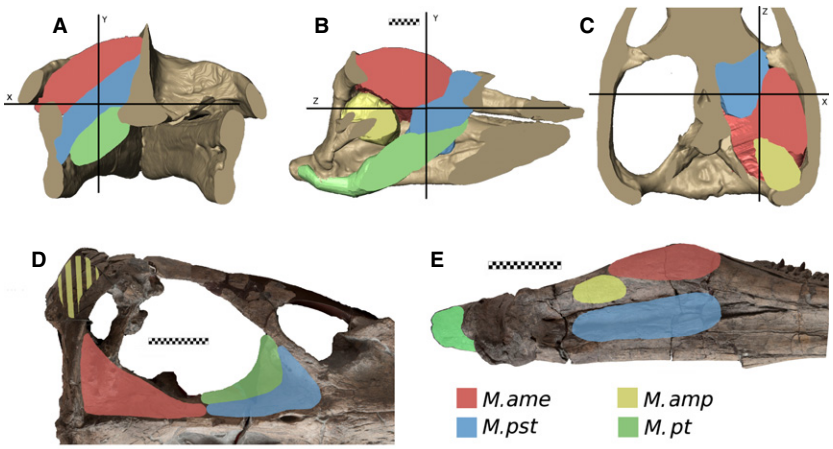

Fig. 2 DORCM G.13 675 Simplified muscle group reconstruction and muscle attachment. (A) Transverse section. (B) Sagittal section. (C) Longitudinal section. (D) Skull adductor muscle attachment sites, dorsal view of the left temporal fossa. (E) Lower jaw adductor muscle attachment sites, medial view of the left mandibular ramus. Scale bar: 10 cm (A–C); 20 cm (D,E).

et al. 2013). For example, broad rostra show greater bending resistance about the dorso-ventral axis (i.e. bending in a mediolateral direction, Iy) than about the medio-lateral axis (i.e. bending in a dorsoventral direction, Ix;Iy ≫ Ix). As a consequence, such shapes perform well in lateral shaking feeding. When Ix and Iy are summed, they equal the polar moment of inertia J, an indicator of resistance to torsion.

Specimens studied were *P. kevani* (DORCM G 13 675), *Baryonyx walkeri* (NHMUK R9951), *Alligator mississippiensis* (OUVC 9761 (Rowe et al. 1999), *Caiman crocodilus* (FMNH 73711), *Gavialis gangeticus* (NHMUK 2005.1605) and *Crocodylus niloticus* (RVC AN1). Teeth were digitally removed from the CT slices and the alveoli were filled to the level of the alveolar opening on the surface of the bones. In this way the effects of the presence or absence of teeth on bending and torsional resistances were removed and brought up to the same standard. Reptilian snout structure is here assumed to meet all the requirements of beam analyses, namely isotropy and homogeneity of the bone tissues (Cuff & Rayfield, 2013). Only the rostral (anterior) 50% of the snout (defined as the distance between the tip of the anterior end of the premaxillae and the orbits) was included in calculations, as the posterior 50% of the snout was damaged. The same percentage interval was therefore considered for the snouts of the crocodiles. Only an estimated 42% of the total length was used for *Baryonyx*, as the specimen lacked most of the posterior region (skull length estimate from Charig & Milner, 1986; for details refer to Table S1).

Second moments of area Ix, Iy and the polar moment of inertia J were calculated using BONEJ, a plugin of IMAGEJ [http://rsb.info.nih.gov/ij (Abramoff et al. 2004); http://bonej.org/ (Doube et al. 2010)]. To take account of the size differences among taxa and evaluate the simple effect of rostrum shape, each snout portion was rescaled to the length of the pliosaur snout by modifying the resolution of each CT image (Cuff & Rayfield, 2013).

Results

Bite force and muscle reconstruction

A description of each muscle group and its contribution to the total force produced and total volume is provided in Table 1 and Fig. 2 (see also Supporting Information Table S2).

M. adductor mandibulae externus (M. ame): originates from the caudal ridge of the post-temporal fenestra and the caudal lateral wall of the parietal crest. It inserts on an evident muscle attachment area around the edge of the coronoid process. Its line of action is slightly caudally inclined in lateral view and it represents by far the largest muscle mass in this model, accounting for the largest

Fig. 3 FEA model and CT-scans of DORCM G.13 675. (A) Rostrum von Mises stress visualisation. (B) Rostrum suture interpretation; green, pmx-mx; red, pmx-pmx; light-blue, v-mx; orange, v-pmx. Scale bar: 10 cm. (C–H) Lower jaws, von Mises stress visualisation; (C–E), bilateral loads; (F–H), unilateral loads. Arrows indicate the key von Mises stress area caudal to the mandibular symphysis.

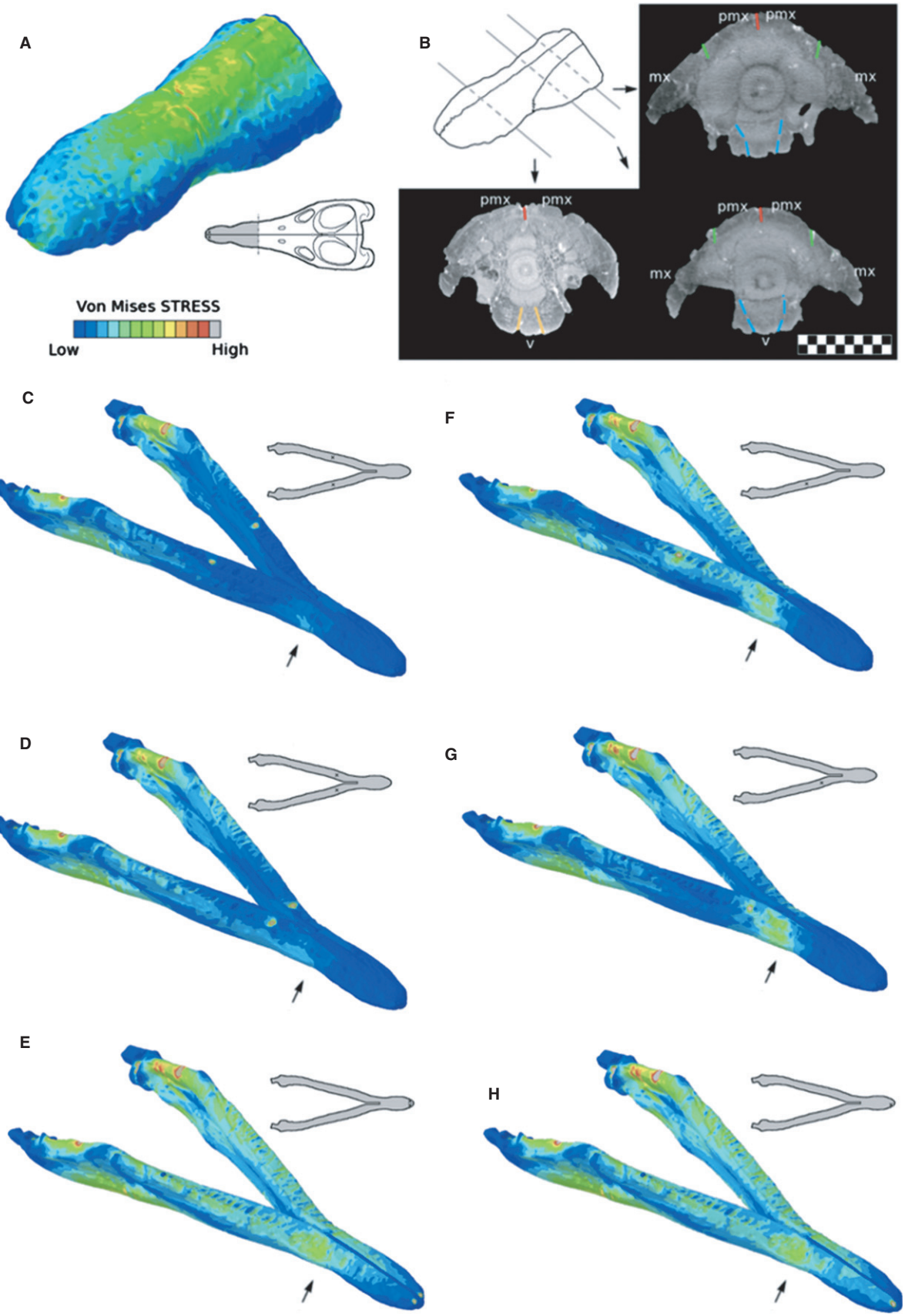

amount of force produced among each muscle group. In our model *M. ame* includes *m. adductor mandibulae externus medialis*; *m. adductor mandibulae externus profundus*; *m. adductor mandibulae externus superficialis*.

M. adductor mandibulae posterior (*M. amp)*: lies ventral to the *M. ame* occupying the posterior ventral area of the temporal fossa. It originates from the anterior surface of the quadrate and the ventrolateral surface face of the reconstructed pterygoid articular process. On the mandible it inserts on a rounded area posterior to the coronoid process on the medial side of the surangular.

M. pseudotemporalis (*M. pst)*: occupies the ventro-anterior part of the temporal fossa. The muscle originates on the reconstructed anterolateral and ventral surface of the sagittal crest, and the posterior wall of the postorbital bar. *M. pst* insertion is the large anteriorly-posteriorly elongated area roughly corresponding to the angular and the prearticular beneath the coronoid process.

M. pterygoideus (*M. pt)*: lies ventral to *M. pst*. It originates from the lateral and ventral side of the pterygoids and a ridge forming the antero-ventral margin of the subtemporal fenestra. It inserts on the articular, posterior to the jaw joint. Our reconstruction of the muscle volume is conservative, and so might have underestimated the real volume; comparisons with modern crocodiles and with McHenry's (2009) model for *K. queenslandicus* suggest that this muscle group might exceed the bone boundary, thus leading to an underestimation of the force produced.

Bite force estimates vary along the tooth row, increasing caudally with reduction in length of the output arm. Magnitudes vary from 9600 to 17 000 N at the anterior dentary tooth to 28 000–48 000 N at the 36th dentary tooth pair (Table 2). When comparing digitally calculated bite forces, our scaling analysis shows that the pliosaur produced bite forces of the same range of the values reported in the available literature for crocodilians and *Kronosaurus* of equal skull length; however, these values are lower than the maximum *in vivo* estimate for *Crocodilus porosus* and *A. mississippiensis* (Table 3) (see Discussion and Data S1, d).

Table 2 Minimum and maximum bite force values.

Biting position	Bite force (min/MAX) [N]	Bite force (min/MAX) [N]
36th dentary	27 685/32 106	41 562/48 728*
23rd dentary	17 497/20 290	26 244/30 795*
13th dentary	13 651/15 830	20 475/24 026*
6th–7th dentary	11 865/13 760	17 797/20 884*
1st dentary/1st premaxillary	9617/11 153	14 425/16 927*

**mpt* rescaled.

Finite element analysis

Rostrum

Models simulating a unilateral and a bilateral bite at the rostral tip show that the highest amount of bite-induced von Mises stress is concentrated on the sagittal line of both ventral and dorsal surfaces (Fig. 3A). The most stressed (von Mises) section corresponds to the caudal end of the premaxillary rosette in line with the maxillary-premaxillary suture. Suture morphology in both the anterior rostrum and the toothed part of the lower jaw is consistent with the FEA results. Different areas of stress and strain occur in line with different kinds of sutures in the skull. The vomer-maxillary and premaxillary caudal contacts are flat or butt-jointed sutures, commonly associated with compressional

Table 3 *Pliosaurus kevani* reaction bite forces compared with other taxa.

Taxon	Method	Bite force range (N)	Skull length [m]	Source
Pliosaurus kevani (min)	Dry skull (3D)	9617/32 106	2	This paper
Pliosaurus kevani (MAX)	Dry skull (3D)	14 425/48 278	2	This paper
Kronosaurus queenslandicus	Dry skull (3D)	15 169/27 716	1.87	McHenry (2009)
Deinosuchus	Scaling from *in vivo* measurements	103 803*	1.85	Erickson et al. (2012)
Crocodylus porosus	*In vivo* measurements	11 216/16 414* (caniniform/ molariform)	0.65	Erickson et al. (2012)
Pliosaurus kevani	Dry skull (3D)	1744/5021	0.65	This paper
Pliosaurus kevani	Dry skull (3D)	990/2851	0.5	This paper
Kronosaurus queenslandicus	Dry skull (3D)	1011/1847	0.48	McHenry (2009)
Crocodylus porosus	Dry skull (3D)	899/1880	0.43	McHenry (2009)
Alligator missippiensis	*In vivo* measurements	9452*	0.48	Erickson et al. (2003)
Alligator missippiensis	MDB	9800/13 135*	0.53	Bates & Falkingham (2012)
Alligator missippiensis	MDB	1400	0.53	Bates & Falkingham (2012)

*bite force peaks.

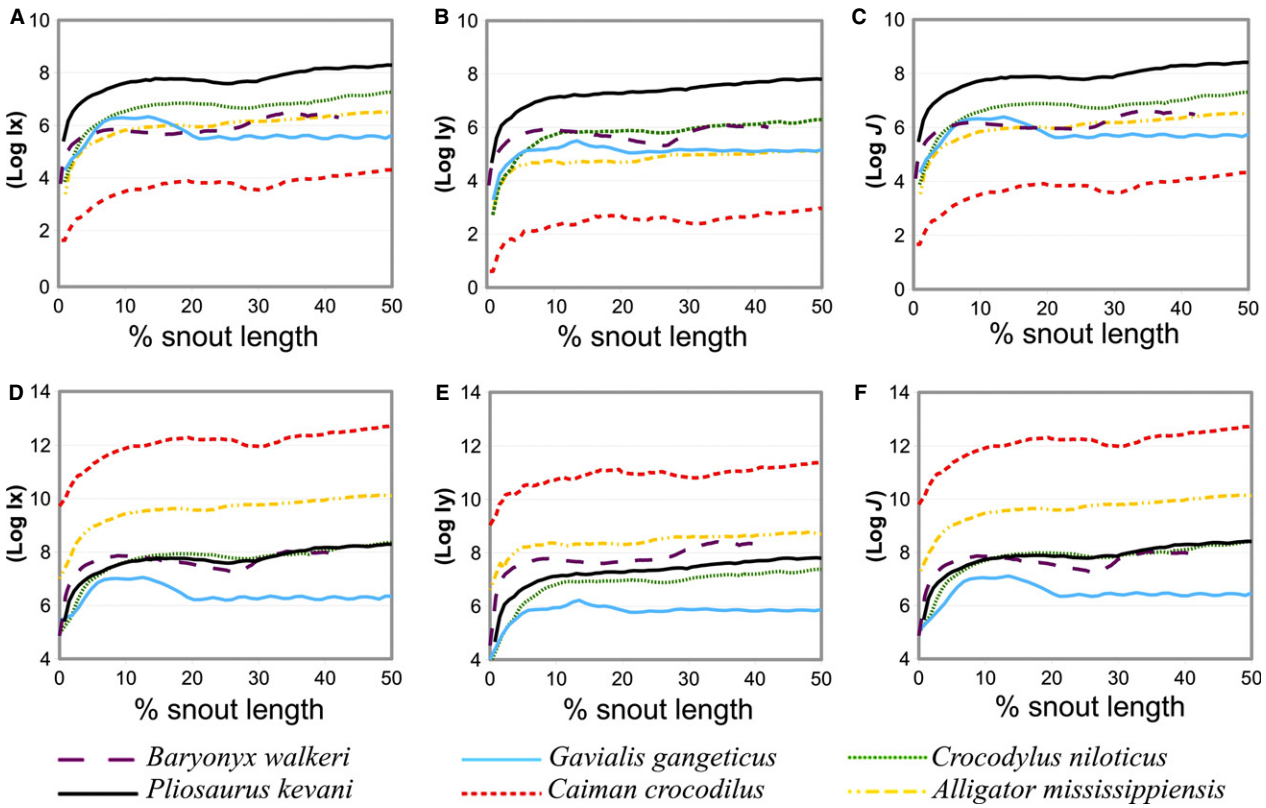

Fig. 4 Second moment of area (I) and polar moment of inertia (J) of crocodilian, spinosaurid and DORCM G.13 675 snouts. (A–C) Absolute value patterns are reported on a logarithmic scale. (D–F) Size-corrected trends obtained by rescaling each snout to the length of the pliosaur. *Ix*, bending resistance about dorso-ventral axis; *Iy*, bending resistance about medio-lateral axis; *J*, tosional resistance (*Ix* + *Iy*).

regimes (L. F. Noè, unpubl. comm.; Rayfield, 2007; M. Gómez-Pérez, unpublished communication). On the terminal rosette, the suture is interdigitate, matching a change into a tensile stress regime. The maxillary-premaxillary contact is an overlapping suture, which provides resistance to bending, tension and twisting forces (Busbey, 1995; M. Gómez-Pérez, unpublished communication). On the lateral side there is substantial interdigitation. Bilateral and unilateral stresses do not differ significantly, as seen also in thalattosuchians (Pierce et al. 2009) with their narrow snouts and rostrally positioned loads.

Lower jaw

In both rami, von Mises stresses are higher for symphyseal bite positions (Fig. 3E,H) than rear and mid tooth row bites (Fig. 3C,D,F,G, respectively). Unilateral and bilateral models show different patterns, but in all models the most stressed area is located at the caudal mandibular symphysis (Fig. 3C–H) (see Data S1, e, Figs S2 and S3).

Beam theory

Not surprisingly given the size of the pliosaur, absolute values for the second moment of area and polar moment of inertia are from one to five orders of magnitude higher than any other taxa considered here. Dorso-ventral (Ix) and medio-lateral (Iy) moments of area and polar moments of inertia (J) show a steady increase towards the caudal rostrum (Fig. 4A–C).

In the size-corrected analyses, pliosaur snout-bending and torsion resistances closely match the mesorostrine *C. niloticus* and the theropod *B. walkeri* (Fig. 4D–F). The pliosaur rostrum shows values higher than the longirostrine *G. gangeticus* but considerably lower than the mesorostrine latirostrine *A. mississippiensis* and *C. crocodilus* (see Data S1,c).

Discussion

Taken together, our study of bite force estimates, beam theory and FEA suggest an animal that was capable of generating strong bite forces but with a relatively 'weak' skull configuration when corrected for size and when compared with contemporary and other fossil aquatic predators. This provides support for previous suggestions about *P. westburyensis* and *Kronosaurus* (Taylor & Cruickshank, 1993; McHenry, 2009).

Bite forces

In spite of its relatively 'weak' skull structure, *P. kevani* is an extremely large animal and is nevertheless well suited for macrophagy. Direct evidence for this comes from morphological features of the specimen such as large tooth sockets (hosting large trihedral teeth), the proportion of the snout, which is wider than tall, and the proportionally short symphysis compared with other pliosaurs such as *Marmornectes* and *Peloneustes* (Tarlo, 1960; Taylor & Cruickshank, 1993; M. Gómez-Pérez, unpubl. comm.; McHenry, 2009; Ketchum & Benson, 2011a,b; Sassoon et al. 2012; Young et al. 2012). Crocodilian symphyseal length can be related to the relative dimensions of prey items (Pierce et al. 2008; Young et al. 2012; Walmsley et al. 2013); by analogy it may be assumed that *P. kevani* prey items were not only absolutely, but also proportionally, larger than those of narrow-snouted pliosaurs.

To our knowledge, the only study on pliosaur bite force was produced by McHenry (2009) and it is based on *Kronosaurus* (1.85 m skull length). The values for *P. kevani* along the tooth row closely match those previously reported in *Kronosaurus* (McHenry, 2009); the differences (lower rostral and higher caudal values) likely arise from features such as snout length and outlever arm length (due to different positions of the most caudal bite position between the two taxa). The bite forces in this study are among the highest inferred in the fossil record, and support the capability of capturing and possibly processing large prey and large bones. Our estimates are commensurate with the highest estimated terrestrial bite forces of 35 000–57 000 N at a single posterior tooth for *Tyrannosaurus rex* (Bates & Falkingham, 2012) and exceed previous high bite force estimates from the marine realm of 5363 N for a 6-m-long *Dunkleosteus* placoderm fish (Anderson & Westneat, 2007) and 9320–18 216 N for the largest white shark, but they are much lower than the estimated 93 127–182 201 N for the extinct shark *Megalodon* (Wroe et al. 2008).

When size is taken into account, the bite forces estimated for *P. kevani* rescaled to 50 cm dorsal cranial length bracket the values calculated in an analogous way for *C. porosus* and *Kronosaurus* (McHenry, 2009). They are also close to multibody dynamics analysis estimates (MDA) of an *A. mississippiensis* sustained bite, the plateau phase in which the force is steady, as opposed to the impact phase where a peak is generated (Bates & Falkingham, 2012) (Table 3). However, these values are significantly lower than the highest peaks of *in vivo* measurements for some crocodilians in Erickson et al. (2012) and the peak MDA values for *Alligator* (Bates & Falkingham, 2012). Some values recorded by Erickson et al. (2012) are impressively high (Table 3); for example, a 4.59-m-long *C. porosus* (roughly 65-cm-long skull) produces a peak *in vivo* bite of 11 000 N at the caniniform teeth, compared with the 2000 N estimate for *P. kevani* rescaled to similar length. Erickson et al. (2012) also estimated a maximum of 103 000 N bite force for *Deinosuchus* (1.8 m mandibular length), much higher than our values for *Pliosaurus*, with a comparable skull length.

This mismatch between *in vivo* and digitally calculated bite forces can be explained in various ways:

1 Crocodilians generate higher bite forces at similar sizes.
2 Erickson et al. (2012) recorded the highest values, presumably produced during impact peaks; in this regard, it was noticed that sustained bites are considerably lower than static values (see also Bates & Falkingham, 2012; Fig. 2) and our models better represent static conditions. If confirmed, this would mean that the values are representative of different situations, and so caution is recommended when comparing them; it would also explain why other digitally calculated values (*Kronosaurus, Crocodylus* and *Alligator*) (McHenry, 2009; Bates & Falkingham, 2012) are comparable with our rescaled model and much lower than Erickson's values.
3 Our correction for pennation is not enough. It might be that crocodilians have more pennate muscles than pliosaurs do, or vice versa.
4 As previously discussed, *M. pt* (*ventralis)* is unconstrained by the lower jaw bones in most lepidosaurs, birds and crocodiles; the extent of this muscle cannot be ascertained for the pliosaur. Hence our model and correction for *M. pt* muscle might still underestimate its volume (see Data S1,b).

To test hypotheses 1 and 2, more comparative studies and further data, ideally from other specimens, would be needed. Hypothesis 2 could also be resolved by using MDB techniques to estimate impact bite peaks or more data on sustained bite for crocodilians taxa; unfortunately, with current knowledge, there is no way to assess hypotheses 3 and 4.

'Weak' skull structure

As in crocodiles, the dimensions of the akinetic pliosaur skull pose a physical limit to the size of prey. In DORCM G.13 675 this limit is quantifiable at approximately 70–80 cm, the distance between the left and right articular surfaces or between the left and right quadrates. In a very conservative case, a prey item of 50–60 cm diameter could theoretically have been swallowed without being seized. Larger pieces must have been somehow processed. Our FE and beam theory analyses underline that the skull lacks specific reinforced structural adaptations; the architecture is functionally analogous to mesorostrine crocodiles (in this case represented by the genus *Crocodylus*), as already demonstrated in *Kronosaurus* (McHenry, 2009). The pliosaur snout is, in fact, more resistant to bending and torsional loads than the rescaled *Gavialis*, but considerably less resistant than either the *Alligator* or the *Cai-*

man. A less demanding alternative to shake and twist feeding is represented by preferential biting at the large post-symphyseal teeth, as observed in many modern crocodilians. After capture, prey could be repositioned with a series of inertial bites and then killed by powerful crushing bites, in line with the large median teeth. This cycle is repeated until the prey item is killed and the mechanical resistance of prey is weakened (Cleuren & De Vree, 2000). However, this explanation, other than being mechanically more advantageous, is supported by limited behavioural evidence.

Pliosaurs were subject to different environmental pressures than extant crocodiles; the necessity of performing quick movements with a long rostrum is a key factor for aquatic taxa. Variation in length, ΔL, triggers a square variation in area ΔA: $\Delta L \propto \Delta A^2$. It follows that the proportionally longer snout, as seen in pliosaurs, causes a quadratically stronger drag than a shorter one; thus a much higher adducting force is required to shut and move the jaws (McHenry et al. 2006; McHenry, 2009). In the same context, an increase in size generally leads to higher absolute resistances; it follows that a relatively 'weak' structure can be comparably the strongest because of its large size, as is shown in Fig. 4.

Our analyses suggest that particularly in the largest pliosaurs, the reduction in relative resistance to bending and torsion is perhaps linked to an increased hydrodynamic agility, as previously suggested in *Pliosaurus* and *Rhomaleosaurus* (Taylor, 1992; Taylor & Cruickshank, 1993); at the same time this structural compromise is counter-balanced by large overall dimensions.

Independent evidence for diet

The extremely large sizes reached by some pliosaurs (up to 12–13 m), suggest little dietary specialisation might be expected (Taylor, 1992; Taylor & Cruickshank, 1993; McHenry, 2009). Their diets and preferred environments may have shifted at different ontogenetic stages (Patterson, 1975; Clarke & Etches, 1992; Taylor et al. 1993; Wiffen et al. 1995), following morphological and size variations, as in most crocodiles (Cleuren & De Vree, 2000).

With the exception of *Leedsichthys*, the species of *Pliosaurus* and two adult-sized crocodilian taxa (*Machimosaurus* and *Plesiosuchus*), the Kimmeridgian fauna is represented by animals considerably smaller than DORCM G.13 675 (Wiffen et al. 1995; Pierce et al. 2009; Benson et al. 2013). Were all of these animals possible prey? Fossilised stomach contents show that cephalopods represented a significant part of the pliosaur diet (Massare, 1987; Martill et al. 1994). Fish remains such as teleosts and hybodont sharks have also been recovered; the reptilian biota from the Kimmeridgian in the UK consists of turtles, thalattosuchian crocodiles, ichthyosaurs and plesiosaurs (Benton & Spencer, 1995; Cruickshank et al. 1996; Sassoon et al. 2010; Knutsen, 2012; Benson et al. 2013), of which several have been shown to be plausible prey for other pliosaur taxa (Tarlo, 1959; Patterson, 1975; Wahl, 1998). Dinosaur dermal elements were found as stomach contents in *Pliosaurus* (Taylor et al. 1993), and fragments of a small (70 cm for 20 kg) turtle, and a plesiosaurian torso were recovered from two specimens of *K. queenslandicus* (McHenry, 2009). Bite marks on plesiosaurian propodials, on the skull of *Eromangasaurus* (a large elasmosaurid about 7 m long and weighing 1–2 tonnes), and on the skull of a small *Kronosaurus,* provide further evidence of active predation by large pliosaurs (Andrews, 1910; Clarke & Etches, 1992; Thulborn & Turner, 1993; Kear, 2005; McHenry, 2009) (see Data 1, f, Table S3, Fig. S4).

Conclusions

Morphology, fossil evidence, FEA, beam theory and bite force estimation concur in describing a powerful unspecialised predator at the apex of the Kimmeridgian marine trophic web. The striking contrast of a comparatively 'weak' skull structure that is poorly adapted to resist bending and twisting loads, and high bite forces, is achieved by increased size and is accounted for by the trade-off between agility and strength in underwater environments. The combination of the hydrodynamic structure of the skull, robust teeth, powerful adductor musculature and large dimensions allowed this animal to prey upon most of the taxa up to half of its own length in the Kimmeridgian seas, thereby providing an insight into Late Jurassic marine ecosystem trophic structure.

Acknowledgements

We particularly thank Colin McHenry for supplying us with unpublished data which considerably contributed to this project; University of Bristol Palaeobiology department staff for advice and help; the University of Southampton and staff involved in the process of CT scanning; DORCM G.13 675; RVC AN1 (*C. niloticus*) was donated by La Ferme aux Crocodiles to John Hutchinson of the Royal Veterinary College, London, and we thank Stephanie Pierce for providing the scan data used here. We thank Tim Rowe and the Digital Morphology Center at the University of Texas for providing scans of FMNH 73711 (*C. crocodilus*). We thank Richard Forrest, Richard Edmonds, Mark Evans, and Roger Benson for useful suggestions and conversations; and particularly the staff of the Dorset County Museum for their kind hospitality during every visit to study the specimen. We are really grateful to Patrick Clarke for the access to his collection. We thank the anonymous reviewers whose comments considerably improved the quality of a previous version of this paper. We are also grateful to the Bob Savage Memorial Fund for enabling visits to the Dorset Museum. We are above all grateful to Kevan Sheehan, the initial discoverer of the specimen, and to Richard Edmonds of the Jurassic Coast project for ensuring all traceable portions of the specimen were retrieved and lodged in the Dorset County Museum.

References

Abramoff MD, Magelhaes PJ, Ram SJ (2004) Image processing with ImageJ. *Biophotonics Int* **11**, 36–42.

Anderson PSL, Westneat MW (2007) Feeding mechanics and bite force modelling of the skull of *Dunkleosteus terrelli*, an ancient apex predator. *Biol Lett* **3**, 76–79.

Andrews CW (1910) *A Descriptive Catalogue of the Marine Reptiles of the Oxford Clay Based on the Leeds Collection in the British Museum (Natural History), London, part I*. London: British Museum (Natural History). xvii + 205 p.

Bates K, Falkingham P (2012) Estimating maximum bite performance in *Tyrannosaurus rex* using multi-body dynamics. *Biol Lett* **8**, 660–664.

Benson RJ, Evans M, Smith AS, et al. (2013) A giant pliosaurid skull from the Late Jurassic of England. *PLoS ONE* **8**, e65989.

Benton MJ (2010) Studying function and behavior in the fossil record. *PLoS Biol* **8**, e1000321.

Benton MJ, Spencer PS (1995) *Fossil Reptiles of Great Britain*. Joint Nature Conservation Committee, Geological Review Series, Vol. 10. London: Chapman & Hall.

Bright J, Rayfield E (2011) The response of cranial biomechanical finite element models to variations in mesh density. *Anat Rec* **294**, 610–620.

Buchy M (2003) First occurrence of a gigantic pliosaurid plesiosaur in the late Jurassic (Kimmeridgian) of Mexico. *Bull Soc Geol Fr* **174**, 271–278.

Busbey AB (1995) The structural consequences of skull flattening in crocodilians. In: *Functional Morphology in Vertebrate Paleontology* (ed. Thomason JJ), pp. 173–192. Cambridge: Cambridge University Press.

Clarke JB, Etches SM (1992) Predation amongst Jurassic marine reptiles. *Proc Dorset Nat Hist Archaeol Soc* **113**, 202–205.

Cleuren J, De Vree F (2000) Feeding in crocodilians. In: *Feeding: Form, Function, and Evolution in Tetrapod Vertebrates* (ed. Schwenk K), pp. 337–358, San Diego: Academic Press.

Cruickshank A, Martill DM, Noé LF (1996) A pliosaur (Reptilia, Sauropterygia) exhibiting pachyostosis from the Middle Jurassic of England. *J Geol Soc* **153**, 873–879.

Cuff AR, Rayfield E (2013) Feeding mechanics in spinosaurid theropods and extant crocodilians. *PLoS ONE* **8**, e65295.

Doube M, Klosowski M, Arganda-Carreras I, et al. (2010) BoneJ Free and extensible bone image analysis in ImageJ. *Bone* **47**, 1076–1079.

Dumont ER, Grosse IR, Slater GJ (2009) Requirements for comparing the performance of finite element models of biological structures. *J Theor Biol* **256**, 96–103.

Erickson GM, Gignac PM, Steppan SJ, et al. (2012) Insights into the ecology and evolutionary success of crocodilians revealed through bite-force and tooth-pressure experimentation. *PLoS ONE* **7**, e31781.

Falkingham P (2012) Acquisition of high resolution three-dimensional models using free, open-source, photogrammetric software. *Palaeontol Electron* **15**, 1–15.

Gorniak GC, Rosenberg HI, Gans C (1982) Mastication in the tuatara, *Sphenodon punctatus* (Reptilia: Rhynchocephalia): structure and activity of the motor system. *J Morphol* **171**, 321–353.

Holliday C (2009) New insights into dinosaur jaw muscle anatomy. *Anat Rec* **292**, 1246–1265.

Holliday C, Witmer L (2007) Archosaur adductor chamber evolution: integration of musculoskeletal and topological criteria in jaw muscle homology. *J Morphol* **268**, 457–484.

Jones MEH, Curtis N, Evans SE, et al. (2009) The head and neck muscles associated with feeding in Sphenodon (Reptilia: Lepidosauria: Rhynchocephalia). *Palaeontol Electron* **12**, 1–56.

Kear BP (2005) A new elasmosaurid plesiosaur from the Lower Cretaceous of Queensland, Australia. *J Vert Paleontol* **25**, 792–805.

Ketchum H, Benson RBJ (2010) Global interrelationships of Plesiosauria (Reptilia, Sauropterygia) and the pivotal role of taxon sampling in determining the outcome of phylogenetic analyses. *Biol Rev* **85**, 361–392.

Ketchum HF, Benson RBJ (2011a) The cranial anatomy and taxonomy of *Peloneustes philarchus* (Sauropterygia, Pliosauridae) from the Peterborough Member (Callovian, Middle Jurassic) of the United Kingdom. *Palaeontology* **54**, 639–665.

Ketchum HF, Benson RBJ (2011b) A new pliosaurid (Sauropterygia, Plesiosauria) from the Oxford Clay Formation (Middle Jurassic, Callovian) of England: evidence for a gracile, longirostrine grade of Early-Middle Jurassic pliosaurids. *Spec Pap Palaeontol* **86**, 109–129.

Knutsen EM (2012) A taxonomic revision of the genus *Pliosaurus* (Owen, 1841a) Owen, 1841b. *Norw J Geol* **92**, 259–276.

Knutsen EM, Druckenmiller PS, Hurum JH (2012) A new species of *Pliosaurus* (Sauropterygia: Plesiosauria) from the Middle Volgian of central Spitsbergen, Norway. *Norw J Geol* **92**, 235–258.

Lautenschlager S (2013) Cranial myology and bite force performance of *Erlikosaurus andrewsi*: a novel approach for digital muscle reconstructions. *J Anat* **222**, 260–272.

Martill D, Taylor M, Duff K, et al. (1994) The trophic structure of the biota of the Peterborough Member, Oxford Clay Formation (Jurassic), UK. *J Geol Soc* **151**, 173–194.

Massare JA (1987) Tooth morphology and prey preference of Mesozoic marine reptiles. *J Vert Paleontol* **7**, 121–137.

McHenry CR (2009) 'Devourer of Gods' - The palaeoecology of the Cretaceous pliosaur *Kronosaurus queenslandicus*. PhD thesis, Digital theses repository of the University of Newcastle, Newcastle, x + 616 pp, http://hdl.handle.net/1959.13/935911.

McHenry C, Clausen P, Daniel W, et al. (2006) Biomechanics of the rostrum in crocodilians: a comparative analysis using finite-element modeling. *Anat Rec* **288A**, 827–849.

Patterson C (1975) The braincase of pholidophorid and leptolepid fishes, with a review of the actinopterygian braincase. *Philos Trans R Soc Lond B Biol Sci* **269**, 282–283.

Pierce S, Angielcyzk K, Rayfield E (2008) Patterns of morphospace occupation and mechanical performance in extant crocodilian skulls: a combined geometric morphometric and finite element modeling approach. *J Morphol* **269**, 840–864.

Pierce S, Angielczyk K, Rayfield E (2009) Morphospace occupation in thalattosuchian crocodylomorphs: skull shape variation, species delineation and temporal patterns. *Palaeontology* **52**, 1057–1097.

Porro L, Holliday C, Anapol F, et al. (2011) Free body analysis, beam mechanics, and finite element modeling of the mandible of *Alligator mississippiensis*. *J Morphol* **272**, 910–937.

Rayfield EJ (2007) Finite element analysis in vertebrate morphology. *Annu Rev Earth Planet Sci* **35**, 541–576.

Rayfield EJ, Norman DB, Horner C, et al. (2001) Cranial design and function in a large theropod dinosaur. *Nature* **409**, 1033–1037.

Reed DA, Porro LB, Iriarte-Diaz J, et al. (2011) The impact of bone and suture material properties on mandibular function in *Alligator mississippiensis*: testing theoretical phenotypes with finite element analysis. *J Anat* **218**, 59–74.

Romer AS (1956) *Osteology of the Reptiles*, pp. 772, Chicago: University of Chicago Press.

Rowe T, Brochu CA, Colbert MW, et al. (1999) Introduction to *Alligator*: digital atlas of the skull. CD-ROM in Society of Vertebrate Paleontology Memior 6. *J Vert Paleontol* **19**, 1–8.

Sassoon J, Vaughan R, Carpenter S, et al. (2010) The second Westbury pliosaur: excavation, collection and preparation. *Geol Curator* **3**, 117–126.

Sassoon J, Noè LF, Benton MJ (2012) Cranial anatomy, taxonomic implications and palaeopathology of an Upper Jurassic Pliosaur (Reptilia: Sauropterygia) from Westbury, Wiltshire, UK. *Palaeontology* **55**, 743–773.

Snively E, Anderson PSL, Ryan MJ (2010) Functional and ontogenetic implications of bite stress in arthrodire placoderms. *Kirtlandia* **57**, 53–60.

Tarlo LB (1959) *Stretosaurus* gen. nov., a giant pliosaur from the Kimmeridge Clay. *Palaeontology* **2**, 39–55.

Tarlo B (1960) A review of the Upper Jurassic pliosaurs. *Bull Br Mus Nat Hist Geol* **4**, 145–189.

Taylor M (1987) How tetrapods feed in water: a functional analysis by paradigm. *J Linn Soc Zool* **91**, 171–195.

Taylor MA (1992) Functional anatomy of the head of the large aquatic predator *Rhomaleosaurus zetlandicus* (Plesiosauria, Reptilia) from the Toarcian (Lower Jurassic) of Yorkshire, England. *Proc R Soc Lond B* **335**, 247–280.

Taylor MA, Cruickshank A (1993) Cranial anatomy and functional morphology of *Pliosaurus brachyspondylus* (Reptilia, Plesiosauria) from the Upper Jurassic of Westbury, Wiltishire. *Philos Trans R Soc Lond B Biol Sci* **341**, 399–418.

Taylor MA, Norman DB, Cruickshank ARI (1993) Remains of an ornithischian dinosaur in a pliosaur from the Kimmeridgian of England. *Palaeontology* **36**, 357–360.

Thomason JJ (1991) Cranial strength in relation to estimated biting forces in some mammals. *Can J Zool* **69**, 2326–2333.

Thulborn RA, Turner S (1993) An elasmosaur bitten by a pliosaur. *Mod Geol* **18**, 489–501.

Wahl W (1998) Plesiosaur gastric contents from the upper Redwater Shale (lower Oxfordian) of the Sundance Formation (Jurassic) of Wyoming. *J Vert Paleontol* **18**, 1–84.

Walmsley CW, Smits PD, Quayle MR, et al. (2013) Why the long face? The mechanics of mandibular symphysis proportions in crocodiles. *PLoS ONE* **8**, 1–34, e53873.

Wiffen J, De Buffrénil V, De Ricqlés A, et al. (1995) Ontogenetic evolution of bone structure in Late Cretaceous Plesiosauria from New Zealand. *Geobios* **28**, 625–640.

Wroe S, Huber D, Lowry M, et al. (2008) Three-dimensional computer analysis of white shark jaw mechanics: how hard can a great white bite? *J Zool* **276**, 336–342.

Young MT, Brusatte SL, De Andrade MB, et al. (2012) The cranial osteology and feeding ecology of the metriorhynchid crocodylomorph genera *Dakosaurus* and *Plesiosuchus* from the Late Jurassic of Europe. *PLoS ONE* **7**, 1–42, e44985.

Zapata U, Metzger K, Wang Q, et al. (2010) Material properties of mandibular cortical bone in the American alligator, *Alligator mississippiensis*. *Bone* **46**, 860–867.

Supporting Information

Additional Supporting Information may be found in the online version of this article:

Data S1. Supporting Information.

Table S1. Detail of the CT scan material for each specimen.

Table S2. Geometrical details of adductor muscle groups.

Table S3. Body length-volume (mass) relationships data.

Fig. S1. Schematic reconstruction of DORCM G 13 675 form the digital model.

Fig. S2. FEA model of DORCM G 13 675 working ramus in unilateral loads.

Fig. S3. Schematic representation of working and balancing side during unilateral load.

Fig. S4. Kimmeridgian marine reptile fauna, dimensions and mass.

Fig. S5. Pliosauridae indet.